

Nonlinear Time-Domain Performance Model for a Wave Energy Converter in Three Dimensions

Ryan G. Coe and Diana L. Bull

Water Power Technologies

Sandia National Labs

Albuquerque, NM 87185-1124

Email: rcoe@sandia.gov, dlbull@sandia.gov

Abstract—A nonlinear three-dimensional time-domain performance model has been developed for a floating axisymmetric point absorbing WEC. This model employs a set of linear partial differential equations, in the form of a state-space model, to replace the convolution integrals needed to solve for radiation reaction. Linear time-domain results are verified against predictions from a frequency-domain model. Nonlinear time-domain predictions are compared back to frequency-domain and linear time-domain predictions to show the effects of some linearization assumptions. A simple resistive control strategy is applied throughout these scenarios.

I. INTRODUCTION

Wave energy converters (WECs) harness the incident power in ocean waves to produce electricity. There are three main methods of power conversion: overtopping devices, oscillating water columns, and wave activated bodies. In each of these methods, a structure interacts with the incident waves: in the case of an overtopping device a reservoir is used to store water that will then run through a turbine to produce energy; an oscillating water column device contains a moonpool with an enclosed air chamber vented to atmosphere through a turbine; wave activated bodies are structures that directly interact with the incident waves, resulting in kinetic motion. A performance model can be employed to study the dynamics and power absorption of a WEC. In addition to the complex hydrodynamics of floating body in irregular waves, such a model must account for the influence of a power conversion chain (PCC), which may exhibit an arbitrary control input as well as stroke and force limitations.

The wave-structure interaction is often modeled using potential flow boundary element method (BEM) solvers. Potential flow is based on linear wave theory and the principle of superposition. Employing these assumptions, BEM codes can solve for a body's radiation and excitation reactions, the former due to the motion of the body in calm seas and the latter due to the effect of waves on a stationary body. Small amplitude motions of the body when subject to waves can be determined with a hydrodynamic equation of motion that includes the superposition of the excitation, radiation, and hydrostatic restoring forces.

The frequency-dependent hydrodynamic terms obtained from a BEM code can be transitioned to the time-domain using the (complex) inverse Fourier transform. Both the excitation and radiation hydrodynamic forces are frequency-dependent and hence possess a corresponding impulse response function (IRF) that must be identified. The convolution of these IRFs

with their respective time-dependent multipliers (free surface elevation and structure velocity) results in time-domain estimations of their effects. A set of linear partial differential equations, represented by a state-space model, have been shown to be an efficient alternative to direct computation of these convolution integrals.

A WEC can be viewed as a coupled hydrodynamic-mechanical-electrical system, as the motion of the device affects power production and the configuration of the PCC can similarly affect rigid-body dynamics. A WEC's PCC is simultaneously capable of increasing a device's performance through dynamic control, while also potentially decreasing the performance through limitations placed on stroke length (in the case of translational conversion) or rotation rate (in the case of rotational conversion). Further, limitations on the maximum allowable force (or torque) produced by a PCC must also be modeled and considered when accurately modeling the performance of a device. Hence, a realistic performance model must incorporate both of these strong influences to accurately predict absorbed power.

This paper explores the development and configuration of a time-domain performance model for a specific WEC of interest. Section II describes the WEC, its geometric characteristics and mode of operation. The theoretical framework and implementation of frequency- and time-domain performance models for this WEC are discussed in Section III. Section IV presents the results from a series of analyses focused on the effects of changes in model configuration. Conclusions from the study and suggestions for future work are discussed in Section V.

II. DEVICE GEOMETRY

This study focuses on the dynamic analysis of an axisymmetric point absorbing WEC, referred to herein as the planar motion point absorber (PMPA), shown in Fig. 1. The PMPA is designed for use in a series numerical and physical (model-scale) tests sponsored by the U.S. Department of Energy to study the implementation and effectiveness of PCC control strategies. The axisymmetric float is connected to ground via a vertical PCC arm, located above the float. The top mount of the PCC is restricted to translate in the horizontal plane. A spring restoring force is applied to this translation thus mimicking the effect of a mooring system on the device. A two-axis universal joint, located at the center of gravity of the float, allows for pitch and roll, but not yaw. The device's modes of motion are shown by red arrows in Fig. 1.

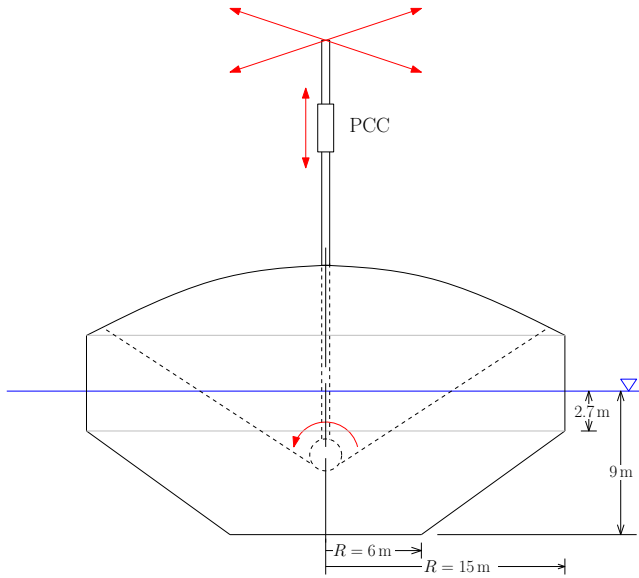


Fig. 1. PMPA geometry and configuration.

TABLE I. RIGID BODY AND GENERAL PROPERTIES OF THE PMPA.

Property, symbol	Value
Mass, m	1.8×10^7 kg
Draft, T	9 m
Radius, r	15 m
Center-of-gravity, $[x_G, y_G, z_G]$	[0 0 -4.852] m
Center-of-buoyancy, $[x_B, y_B, z_B]$	[0 0 -3.352] m
Moments-of-inertia, $[I_{xx}, I_{yy}, I_{zz}]$	$[2.12 \ 2.12 \ 3.80] \times 10^8$ kg m ²
Mooring spring constants, $[\mathbf{C}^{m_{11}}, \mathbf{C}^{m_{22}}]$	[31.526 31.526] kN/m
End-stop constants, $[\alpha_{ES}, \beta_{ES}]$	$[7.10 \text{ kN/m } 31.0 \text{ N s/m}] \times 10^5$

Fig. 1 also gives dimensions for the float's submerged geometry. The rigid-body properties of the PMPA were determined assuming a uniform distribution of mass combined with a point mass to lower the center of gravity (COG) below the center of buoyancy (COB). The rigid-body properties of the PMPA are given in Table I. Both the COB and COG locations are reported with respect to the still-water line. (Dimensions in Fig. 1 and Table I, as well as results presented throughout this paper, are given in full-scale.)

Higher-order panels representing the three-dimensional wetted surface of the PMPA were used to model the PMPA's submerged geometry in the BEM potential flow solver WAMIT [1]. Utilizing the device's planes of symmetry ($x = 0$ and $y = 0$), one quarter of the float was modeled using 704 panels.

III. PERFORMANCE MODEL

Both frequency- and time-domain performance models were developed to analyze the dynamic motions and power production of the PMPA. The frequency-domain model serves to verify the implementation of the time-domain model at its most simplified level. (The time-domain model has been implemented using varying levels of complexity, which will be discussed in the subsequent sections.)

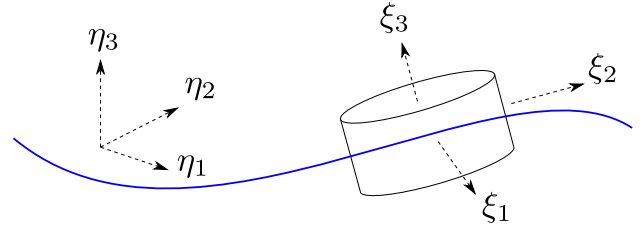


Fig. 2. Inertial and body-fixed coordinate system employed in time-domain model.

A. Coordinate Systems and Transformations

The inertial and body-fixed coordinate systems employed in the models are illustrated in Fig. 2. It is convenient to center the body-fixed coordinate system at the center of gravity. The position and orientation of the float in the inertial frame is given by the vector η .

$$\eta = \begin{bmatrix} \varepsilon \\ \vartheta \end{bmatrix} = \begin{bmatrix} x \\ y \\ z \\ \phi \\ \theta \\ \psi \end{bmatrix} \quad (1)$$

The inertial coordinate system is oriented such that the positions x , y and z correspond to North, West and Up respectively.

Velocities in the body-fixed frame are similarly given by the vector $\dot{\xi}$.

$$\dot{\xi} = \begin{bmatrix} u \\ v \\ w \\ p \\ q \\ r \end{bmatrix} \quad (2)$$

The elements of $\dot{\xi}$ correspond with surge, sway, heave, roll, pitch and yaw velocities respectively. Note that for the PMPA, ψ and r are always zero.

The body's center of buoyancy and gravity can be defined in the body-fixed frame as $r_B = [x_B \ y_B \ z_B]^T$ and $r_G = [x_G \ y_G \ z_G]^T$ respectively. Table I gives the locations of the PMPA's center of buoyancy and gravity.

An Euler angle transformation matrix, $\mathbf{J}(\vartheta)$, can be employed to solve for the change in the float's inertial position (see e.g., [2], [3]).

$$\dot{\eta} = \begin{bmatrix} \dot{\varepsilon} \\ \dot{\vartheta} \end{bmatrix} = \mathbf{J}(\vartheta) \dot{\xi} \quad (3)$$

The transformation matrix $\mathbf{J}(\vartheta)$ is dependent on the rotation order. If a z - y - x order is employed, a singularity occurs at pitch angles of 90° . (A pitch angle of 90° would not be physical for the PMPA, as it is constrained in pitch by its vertical PCC)

arm.) Using this rotation order, $\mathbf{J}(\vartheta)$ can be defined as a block-diagonal matrix.

$$\mathbf{J} = \begin{bmatrix} \mathbf{R}(\vartheta) & \mathbf{0}_{3 \times 3} \\ \mathbf{0}_{3 \times 3} & \mathbf{T}(\vartheta) \end{bmatrix}. \quad (4)$$

For the PMPA, in which no rotation is allowed about the vertical axis ($\psi = 0$), the upper block of the transformation matrix is given as follows.

$$\mathbf{R}(\vartheta) = \begin{bmatrix} c\theta & s\theta s\phi & c\phi s\theta \\ 0 & c\phi & -s\phi \\ -s\theta & c\theta s\phi & c\theta c\phi \end{bmatrix} \quad (5a)$$

$$\mathbf{T}(\vartheta) = \begin{bmatrix} 1 & s\phi t\theta & c\phi t\theta \\ 0 & c\phi & -s\phi \\ 0 & s\phi/c\theta & c\phi/c\theta \end{bmatrix} \quad (5b)$$

In (5), the letters s , c and t represent the trigonometric functions sine, cosine and tangent respectively.

Simplifications to the transformation matrix can be employed to reduce the complexity of the equation of motion. The 1st-order transformation removes the trigonometric dependence resulting in the following component blocks.

$$\mathbf{R}(\vartheta)^{1^{st}} = \begin{bmatrix} 1 & 0 & \theta \\ 0 & 1 & -\phi \\ -\theta & \phi & 1 \end{bmatrix} \quad (6a)$$

$$\mathbf{T}(\vartheta)^{1^{st}} = \begin{bmatrix} 1 & 0 & \theta \\ 0 & 1 & -\phi \\ 0 & \phi & 1 \end{bmatrix} \quad (6b)$$

To allow for comparison with a linear frequency-domain model, the 0th-order formulation of transformation matrix is required. The 0th-order transformation matrix is a 6×6 identity matrix.

B. Time-Domain Model

A time-domain model was developed using the integro-differential formulation introduced by Cummins [4]. The time-domain equations of motion for a floating body can be defined in the body-fixed coordinate system illustrated in Fig. 2 by

$$[\mathbf{M}_{RB} + \mathbf{A}_\infty] \ddot{\xi} + \int_0^t \mathbf{K}_r(t-\lambda) \dot{\xi}(\lambda) d\lambda + \mathbf{J}(\vartheta)^{-1} (\mathbf{G} + \mathbf{C}_m) \eta + \tau_v = \tau_e + \tau_u. \quad (7)$$

Here, \mathbf{M}_{RB} is the rigid-body mass matrix, which is a function of the body mass, m , the center of gravity, r_G and the rigid-body moments of inertia, I_{ij} . At this stage in the development of the model, the mass of the PCC assembly is considered to be negligible; future model versions will address this issue.

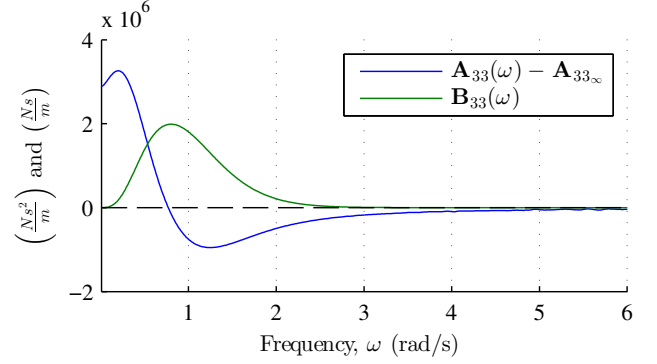


Fig. 3. Frequency dependent added mass, $A_{33}(\omega)$, and damping, $B_{33}(\omega)$, for PMPA float in the heave-heave response.

$$\mathbf{M}_{RB} = \begin{bmatrix} m & 0 & 0 & 0 & -mz_G & -my_G \\ 0 & m & 0 & -mz_G & 0 & -mx_G \\ 0 & 0 & m & my_G & -mx_G & 0 \\ 0 & mz_G & my_G & I_{xx} & I_{xy} & I_{xz} \\ mz_G & 0 & mx_G & I_{yx} & I_{yy} & I_{yz} \\ -my_G & mx_G & 0 & I_{zx} & I_{zy} & I_{zz} \end{bmatrix} \quad (8)$$

Combining (7) and (3), the motion of the body in the inertial frame can be integrated in time. Note that, as (7) employs a non-inertial reference frame, there exist second-order dynamic effects (i.e., Coriolis and centripetal) that are not included in the current formulation. These effects, as well as terms to account for the mass of the PCC assembly, will be included in subsequent versions of this model.

1) *Added-Mass and Radiation Damping*: Fig. 3 shows the added mass, $A_{33}(\omega) - A_{33\infty}$, and damping, $B_{33}(\omega)$, for the PMPA float in the heave-heave response. Here, \mathbf{A}_∞ is the infinite-frequency added mass matrix ($\mathbf{A}_\infty = \mathbf{A}(\omega = \infty)$). The radiation IRF, which is also known as the memory or retardation kernel, can be obtained from either of two inverse Fourier transforms [4], [5]. The velocity-based IRF, \mathbf{K}_r , is given by

$$\mathbf{K}_r(t) = -\frac{2}{\pi} \int_0^\infty \omega [\mathbf{A}(\omega) - \mathbf{A}_\infty] \sin(\omega t) d\omega \quad (9a)$$

$$= \frac{2}{\pi} \int_0^\infty \mathbf{B}(\omega) \cos(\omega t) d\omega. \quad (9b)$$

As $\mathbf{B}(\omega)$ tends to converge to zero more quickly than $A(\omega)$, (9b) is generally preferred for this application.

It can be shown, using Green's theorem (see e.g., [6]), that both the added mass, $\mathbf{A}(\omega)$, and damping, $\mathbf{B}(\omega)$, matrices are symmetric (i.e., $\mathbf{A}_{ij}(\omega) = \mathbf{A}_{ji}(\omega)$). Note that this conclusion is dependent on the assumption of an ideal fluid.

2) *Hydrostatic and Mooring Restoring*: The hydrostatic-gravitational restoring balance is given by the product $\mathbf{G}\eta$. For a body in which the center of gravity and center of buoyancy lie on the same vertical line (i.e., the body is statically stable), \mathbf{G} is a sparse matrix with the nonzero entries

$$\mathbf{G}_{33} = \rho g A_{wp} \quad (10a)$$

$$\mathbf{G}_{44} = \rho g \nabla \left(\frac{S_{22}}{\nabla} + z_B - z_G \right) \quad (10b)$$

$$\mathbf{G}_{55} = \rho g \nabla \left(\frac{S_{11}}{\nabla} + z_B - z_G \right). \quad (10c)$$

Here, ρ gives the density of the water, g gives the acceleration due to gravity and ∇ is the submerged volume of the body. The area of the waterplane is given by A_{wp} while terms S_{ij} are the 2nd-moments of the waterplane area. The terms in the parentheses of (10b) and (10c) are equivalent to the transverse and longitudinal metacentric heights respectively. Note that, for any body with a waterplane area that does not remain constant with draft, the formulation shown in (10) is a linearization.

The mooring-restoring forces are represented by the product $\mathbf{C}_m \eta$. For the PMPA, the mooring system is approximated as linear springs in lateral plane. As such, \mathbf{C}_m is a sparse matrix where only $\mathbf{C}_{m_{11}}$ and $\mathbf{C}_{m_{22}}$ are nonzero with the value given in Table I. Note that to be applied in the body-fixed frame, both the mooring and hydrostatic restoring reactions must be transformed using $\mathbf{J}(\vartheta)^{-1}$.

3) *Viscous Damping*: Viscous damping phenomena are represented in (7) by the variable τ_v . In this study only the linear damping formulation was considered. However, future versions of the time-domain model will incorporate more accurate viscous damping formulations, like the Morison formulation [7]. The linear viscous damping is represented with

$$\tau_v = \mathbf{B}_v^L \dot{\xi}. \quad (11)$$

This formulation uses a constant coefficient matrix \mathbf{B}_v^L . For this study, the elements of \mathbf{B}_v^L were set as a fraction of the critical damping factor.

$$\mathbf{B}_v^L = 2\gamma_v \sqrt{(\mathbf{M}_{RB} + \mathbf{A}_\infty)(\mathbf{G} + \mathbf{C}_m)} \quad (12)$$

This formulation enables the reduction of responses at resonance(s) [8]. The viscous damping constant in (12), γ_v , was set equal to 0.02.

4) *Excitation Reaction*: In the frequency domain, the excitation force can be characterized by the product of the complex excitation response function and wave elevation function.

$$\hat{\tau}_e(\omega) = \hat{\mathbf{H}}(\omega) \hat{\zeta}(\omega) \quad (13)$$

For an a priori known wave history, this formulation can be used to obtain the an excitation force history in the time-domain. For a finite number, N , of component waves, each

with a frequency of $\omega = n\Delta\omega$, (13), the related components of the complex excitation can be written as

$$\hat{\tau}_{e,n} = \hat{\mathbf{H}}_n \hat{\zeta}_n. \quad (14)$$

The time history of the excitation force can be obtained by summing the contribution of N of component waves.

$$\tau_e(t) = \sum_{n=1}^N \Re\{\hat{\tau}_{e,n} e^{i\omega_n t}\} \quad (15)$$

The n^{th} component of the complex wave elevation, with a wave with a frequency of $n\Delta\omega$, can be obtained from the energy density at that frequency, $S_{\zeta,n} = S_{\zeta}(n\Delta\omega)$ and a random phase angle, $\sigma_{\zeta,n}$.

$$\hat{\zeta}_n = \sqrt{2S_{\zeta,n}\Delta\omega} e^{i\sigma_{\zeta,n}} \quad (16)$$

The methodology shown in (14-16) can be applied for a monochromatic wave by setting $N = 1$.

Note that the method described above assumes complete knowledge of the future wave history. An alternative approach, in which this assumption may be relaxed, employs the convolution of a non-causal excitation IRF and the free surface elevation. To implement this approach, the non-causal IRF must be ‘‘causalized’’ (see e.g., [9]).

5) *PCC Reaction and Control Strategy*: The vector τ_u is defined by the reaction imposed by the PCC in the inertial frame, $\tilde{\tau}_u$, along with the current position and orientation of the float.

$$\tau_u = \mathbf{J}(\vartheta)^{-1} \tilde{\tau}_u, \quad (17)$$

where, since the PCC of the PMPA remains vertical at all times, $\tilde{\tau}_u$ can be simply defined by the a scalar, f_u .

$$\tilde{\tau}_u = \begin{bmatrix} 0 \\ 0 \\ f_u \\ 0 \\ 0 \\ 0 \end{bmatrix}. \quad (18)$$

In this study, the PCC reaction is defined by a simple resistive control strategy. Hence, f_u is given by the product of a constant factor, R_{load} , and the extension rate PCC arm, $\dot{\ell}$.

$$f_u = R_{load} \dot{\ell} \quad (19)$$

The PCC extension rate, $\dot{\ell}$, can be determined from change in the float’s inertial position (given by (3)).

$$\dot{\ell} = \dot{z} = \dot{\eta}_3 \quad (20)$$

The power absorbed by the device is the product of the force, f_u , in the PCC and the velocity of PCC arm.

$$p_{abs}(t) = f_u \dot{\ell} = (R_{load} \dot{\ell}) \dot{\ell} \quad (21)$$

An optimal R_{load} can be determined to maximize power absorption. While a numerical optimization is required in irregular spectra, a generic¹ analytic solution exists for the optimal R_{load} in regular waves (see e.g., [10]).

$$R_{load}^{opt} = \frac{\hat{\mathbf{H}}(\omega)}{\left(\mathbf{B}(\omega) + \mathbf{B}_v^L + i\omega(\mathbf{M}_{RB} + \mathbf{A}(\omega) - \frac{\mathbf{G} + \mathbf{C}_m}{\omega^2}) \right)} \quad (22)$$

6) *PCC Constraints*: Two of the constraints typically seen in the operation of real WEC devices, PCC force saturation limits and stroke length limitations, have been applied within the time-domain model.

A PCC force saturation limit was implemented by limiting the force applied by the PCC, τ_u , to a saturation value at τ_u^{max} .

$$\tau_u = \text{sign}(-f_u) \min(|-f_u|, |\tau_u^{max}|) \quad (23)$$

Similarly, a hard limit can be imposed on the extension of the PCC to mimic a physical end-stop. The instantaneous length of the PCC can be defined by

$$\ell = z. \quad (24)$$

The extension of the PCC can thus be defined by the difference from its central position, ℓ_0 .

$$\Delta\ell = \ell - \ell_0 \quad (25)$$

Motion constraints were applied to limit the extension of the PCC ($|\Delta\ell| \leq \Delta\ell_{max}$) following the repulsive potential formulation given by Hals et al. [11].

$$f_{ES} = \text{sign}(\Delta\ell) \alpha_{ES} \gamma h(\gamma) - \beta_{ES} \dot{\ell} h(\gamma) \quad (26)$$

where $\gamma = |\Delta\ell| - \Delta\ell_{max}$

Here, h denotes the Heaviside step function. The constants α_{ES} and β_{ES} are the spring and damping end-stop parameters respectively, which must be tuned to obtain the desired behavior. The values used for this study are given in Table I. The end-stop force, f_{ES} , given by (26), is incorporated in the model following the same means as the resistive PCC reaction (17-18).

¹This is strictly accurate only when no transformation matrix is required to accurately model the device (e.g., a single-degree-of-freedom heave device).

C. Time-Domain Model Numerical Implementation

1) *Radiation and Convolution Replacement*: The presence of a convolution integral in (7) is undesirable, as it is computationally expensive to evaluate and limits the use of analysis and control design methods. For these reasons, it is useful to replace the convolution integrals that appear in (7) with another mathematical model. The computational expense of evaluating the convolution integral is partially driven by the need to store the results from a simulation time step throughout the solution process and use them to re-evaluate the entire convolution integral. This issue is compounded by the fact that for a 6 degree-of-freedom system, there can, in general, exist thirty-six unique IRFs to be convolved.

The most common method used to lessen the numerical cost of evaluating a convolution integral is to replace it by a linear ordinary differential equation (ODE), written as a state-space model (SSM).

$$\left(\mu(t) = \int_0^t \mathbf{K}_r(t-\lambda) \dot{\xi}(\lambda) d\lambda \right) \Leftrightarrow \begin{cases} \dot{x}_r = \mathbf{A}_r x_r + \mathbf{B}_r \dot{\xi}(t) \\ \check{\mu}(t) = \mathbf{C}_r x_r \end{cases}$$

$$\text{where } \begin{matrix} x_r \in R^{n \times 1} & \mathbf{A}_r \in R^{n \times n} \\ \mathbf{B}_r \in R^{n \times 1} & \mathbf{C}_r \in R^{1 \times n} \end{matrix} \quad (27)$$

While the order of system, n , depends on the nature of the specific IRF, radiation IRFs can often be represented by systems with $3 \leq n \leq 8$. The matrices \mathbf{A}_r , \mathbf{B}_r and \mathbf{C}_r must be chosen to produce a vector $\check{\mu}$ to mimic μ . The radiation state vector, x_r , has no direct physical meaning.

An SSM to represent a given IRF can be obtained using methods operating in either the time or frequency domain (see e.g., [12]–[14]). In this study, a time-domain identification was implemented using realization theory [12]. Each non-zero element of the PMPA's radiation kernel matrix, \mathbf{K}_r , was represented with an 8th-order SSM.

For a body with no planes or axes of symmetry (and assuming a real fluid), there exist twenty-one distinct radiation terms that compose a symmetric ($\mathbf{K}_{r,ij} = \mathbf{K}_{r,ji}$) 6×6 matrix, \mathbf{K}_r . Thirty-six convolutions must be evaluated to obtain the radiation reaction $\mu \in \mathfrak{R}^{6 \times 1}$.

$$\mu = \begin{bmatrix} \mu_1 = \sum_{j=1}^6 \mu_{1,j} \\ \mu_2 = \sum_{j=1}^6 \mu_{2,j} \\ \vdots \\ \mu_6 = \sum_{j=1}^6 \mu_{6,j} \end{bmatrix}. \quad (28)$$

If the convolution terms are to be replaced by SSMs, there must exist up to thirty-six sets of SSMs. To reduce complexity and computational load, we can assemble the matrices of these systems into into a single SSM. Taghipour [15] used

such a method without reporting the form of the matrices and Duarte [16] presented a matrix assembly formulation that follows a somewhat different concept.² We will consider the task of assembling a compound SMM in a two step process, as illustrated in Fig. 4.

- 1) Assemble six SSMs such that each element of $\check{\mu}$ can be obtained by evaluating a SSM. The component matrices created by this step of the process are written with square brackets: $[\mathbf{A}_r]^{(i)}$, $[\mathbf{B}_r]^{(i)}$, $[\mathbf{C}_r]^{(i)}$ and $[x_r]^{(i)}$.
- 2) Assemble the SSMs from Step 1 into a single SSM so that the vector $\check{\mu}$ can be obtained by evaluating a single SSM. The component matrices created by this step of the process are written with curly brackets: $\{\mathbf{A}_r\}$, $\{\mathbf{B}_r\}$, $\{\mathbf{C}_r\}$ and $\{x_r\}$

This process can be described as follows:

Step 1 Each element of $\check{\mu}$ can be defined by a single SSM.

$$\begin{aligned} [\dot{x}_r]^{(i)} &= [\mathbf{A}_r]^{(i)}[x_r]^{(i)} + [\mathbf{B}_r]^{(i)}\dot{\xi} \\ \check{\mu}_i &= [\mathbf{C}_r]^{(i)}[x_r]^{(i)} \end{aligned} \quad (29)$$

The $[\mathbf{A}_r]^{(i)}$ matrix can be assembled as a block diagonal of the dimension $\left[\sum_{i=1}^6 n_i \times \sum_{i=1}^6 n_i \right]$.

$$[\mathbf{A}_r]^{(i)} = \begin{bmatrix} \mathbf{A}_r^{(i,1)} & & \mathbf{0} \\ & \ddots & \\ \mathbf{0} & & \mathbf{A}_r^{(i,6)} \end{bmatrix} \quad (30)$$

Here, $\mathbf{A}_r^{(i,j)}$ is the \mathbf{A}_r matrix that corresponds to $\check{\mu}_{i,j}$, with a similar notation for $\mathbf{B}_r^{(i,j)}$, $\mathbf{C}_r^{(i,j)}$ and $x_r^{(i,j)}$. The $[\mathbf{B}_r]^{(i)}$ matrix is a block diagonal of the dimension $\left[\sum_{i=1}^6 n_i \times 6 \right]$.

$$[\mathbf{B}_r]^{(i)} = \begin{bmatrix} \mathbf{B}_r^{(i,1)} & & \mathbf{0} \\ & \ddots & \\ \mathbf{0} & & \mathbf{B}_r^{(i,6)} \end{bmatrix} \quad (31)$$

The matrix $[\mathbf{C}_r]^{(i)} \in \mathfrak{R}^{1 \times 6n}$ is given as a vector of the dimension $\left[1 \times \sum_{i=1}^6 n_i \right]$.

$$[\mathbf{C}_r]^{(i)} = \left[\mathbf{C}_r^{(i,1)} \quad \mathbf{C}_r^{(i,2)} \quad \dots \quad \mathbf{C}_r^{(i,6)} \right]. \quad (32)$$

The state vector $[x_r]^{(i)} \in \mathfrak{R}^{6n \times 1}$ is a vector of the dimension $\left[\sum_{i=1}^6 n_i \times 1 \right]$.

$$[x_r]^{(i)} = \begin{bmatrix} x_r^{(i,1)} \\ x_r^{(i,2)} \\ \vdots \\ x_r^{(i,6)} \end{bmatrix} \quad (33)$$

Step 2 This assembly methodology can be taken one step further to let the vector $\check{\mu}$ be defined by a single SSM.

$$\begin{aligned} \{\dot{x}_r\} &= \{\mathbf{A}_r\} \{x_r\} + \{\mathbf{B}_r\} \dot{\xi} \\ \check{\mu} &= \{\mathbf{C}_r\} \{x_r\} \end{aligned} \quad (34)$$

Here, the SSM's matrices can be given by the following assemblies, shown both in terms of the intermediary $[\mathbf{A}_r]^{(i)}$, $[\mathbf{B}_r]^{(i)}$, $[\mathbf{C}_r]^{(i)}$ and $[x_r]^{(i)}$ matrices and the matrices of the original thirty-six SSMs.

$$\begin{aligned} \{\mathbf{A}_r\} &= \begin{bmatrix} [\mathbf{A}_r]^{(1)} & & \mathbf{0} \\ & \ddots & \\ \mathbf{0} & & [\mathbf{A}_r]^{(6)} \end{bmatrix} \\ &= \begin{bmatrix} \mathbf{A}^{(1,1)} & & \mathbf{0} \\ & \mathbf{A}^{(1,2)} & \\ \mathbf{0} & & \ddots \\ & & & \mathbf{A}^{(6,6)} \end{bmatrix} \end{aligned} \quad (35)$$

$$\begin{aligned} \{\mathbf{B}_r\} &= \begin{bmatrix} [\mathbf{B}_r]^{(1)} \\ [\mathbf{B}_r]^{(2)} \\ \vdots \\ [\mathbf{B}_r]^{(6)} \end{bmatrix} = \begin{bmatrix} \mathbf{B}_r^{(1,1)} & & \mathbf{0} \\ & \ddots & \\ \mathbf{0} & & \mathbf{B}_r^{(1,6)} \\ \vdots & & \vdots \\ \mathbf{B}_r^{(6,1)} & & \mathbf{0} \\ \mathbf{0} & & \ddots & \mathbf{B}_r^{(6,6)} \end{bmatrix} \end{aligned} \quad (36)$$

$$\begin{aligned} \{\mathbf{C}_r\} &= \begin{bmatrix} [\mathbf{C}_r]^{(1)} & & \mathbf{0} \\ & \ddots & \\ \mathbf{0} & & [\mathbf{C}_r]^{(6)} \end{bmatrix} \\ &= \begin{bmatrix} [\mathbf{C}_r^{(1,1)} & \dots & \mathbf{C}_r^{(1,6)} & & \mathbf{0} \\ & & & \ddots & \\ \mathbf{0} & & & & [\mathbf{C}_r^{(6,1)} & \dots & \mathbf{C}_r^{(6,6)}] \end{bmatrix} \end{aligned} \quad (37)$$

²Duarte's formulation relies on the fact that both the added mass, $\mathbf{A}(\omega)$, and damping, $\mathbf{B}(\omega)$, matrices are considered symmetric.

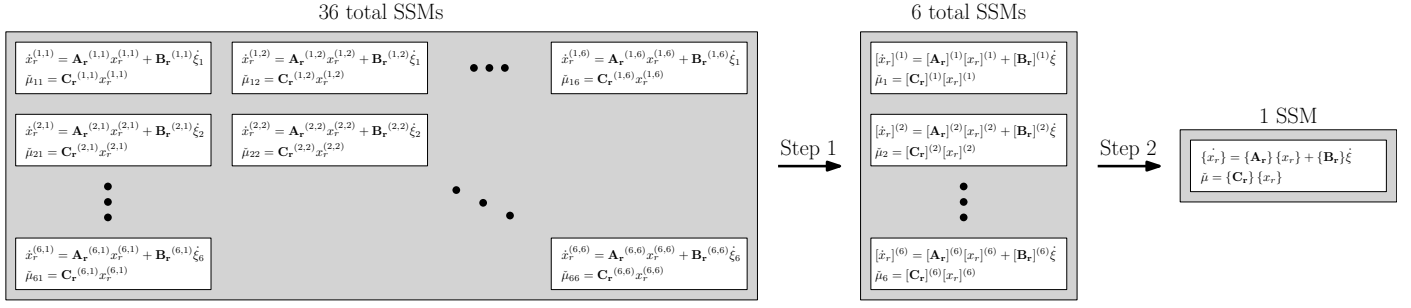


Fig. 4. Multi-degree-of-freedom convolution SSM assembly process: Step 1 moves from one for system for each radiation term (thirty-six) to one system for each response mode (six); Step 2 moves to a single state-space system.

TABLE II. MATRIX DIMENSIONS OF ASSEMBLED MULTI-DEGREE-OF-FREEDOM CONVOLUTION REPLACEMENT SSMs.

Term	Rows	Columns
$\{\mathbf{A}_r\}$	$\sum_{i=1}^6 \sum_{j=1}^6 n_{i,j}$	$\sum_{i=1}^6 \sum_{j=1}^6 n_{i,j}$
$\{\mathbf{B}_r\}$	$\sum_{i=1}^6 \sum_{j=1}^6 n_{i,j}$	6
$\{\mathbf{C}_r\}$	6	$\sum_{i=1}^6 \sum_{j=1}^6 n_{i,j}$
$\{x_r\}$	$\sum_{i=1}^6 \sum_{j=1}^6 n_{i,j}$	1

$$\{x_r\} = \begin{bmatrix} [x_r]^{(1)} \\ [x_r]^{(2)} \\ \vdots \\ [x_r]^{(6)} \end{bmatrix} = \begin{bmatrix} [x_r^{(1,1)}] \\ \vdots \\ [x_r^{(1,6)}] \\ \vdots \\ [x_r^{(6,1)}] \\ \vdots \\ [x_r^{(6,6)}] \end{bmatrix} \quad (38)$$

The dimensions of the matrices defined in (35-38) are given in Table II. The variable $n_{i,j}$ is used here to denote the order of the $(i,j)^{\text{th}}$ state-space model. Thus, for instance, if you had a system in which every radiation term were represented by 3rd-order SSM, the assembled matrices would be of the follow dimensions. Note that each mode may be represented by an SSM of arbitrary order.

$$\{\mathbf{A}_r\} \in \mathfrak{R}^{108 \times 108} \quad \{\mathbf{B}_r\} \in \mathfrak{R}^{108 \times 6}$$

$$\{\mathbf{C}_r\} \in \mathfrak{R}^{6 \times 108} \quad \{x_r\} \in \mathfrak{R}^{108 \times 1}$$

$$\text{where if } n_{i,j} = 3, \sum_{i=1}^6 \sum_{j=1}^6 n_{i,j} = 108 = N$$

2) *System Solution*: Working from the physical system defined by (7), it is convenient to define the states of the model as follows:

$$\begin{aligned} x_{1:N} &= x_r \\ x_{N+1:N+6} &= \eta \\ x_{N+7:N+12} &= \dot{\xi}, \end{aligned} \quad (39)$$

where N is the order of the full radiation SSM. Thus the system state vector can be written as

$$x_{sys} = \begin{bmatrix} \hat{x}_1 \\ \vdots \\ \hat{x}_2 \\ \vdots \\ \hat{x}_3 \end{bmatrix} = \begin{bmatrix} x_r|1 \\ \vdots \\ x_r|N \\ \hline \eta_1 \\ \vdots \\ \eta_6 \\ \hline \dot{\xi}_1 \\ \vdots \\ \dot{\xi}_6 \end{bmatrix}. \quad (40)$$

A system of differential equations for this state vector can be written as

$$\begin{aligned} \hat{x}'_1 &= \{\mathbf{A}_r\} \hat{x}_1 + \{\mathbf{B}_r\} \hat{x}_3 \\ \hat{x}'_2 &= \mathbf{J}(\hat{x}_2) \hat{x}_3 \\ \hat{x}'_3 &= \mathbf{M}^{-1} [\tau_e + \tau_u - (\{\mathbf{C}_r\} \hat{x}_1 + \mathbf{B}_v^L \hat{x}_3 + (\mathbf{G} + \mathbf{C}_m) \hat{x}_2)]. \end{aligned} \quad (41)$$

Here, \mathbf{M} is the sum of the rigid body and added mass matrices ($\mathbf{M} = \mathbf{M}_{RB} + \mathbf{A}_\infty$). For an arbitrary excitation, τ_e , (41) can be advanced in time via numerical integration. This was accomplished in MATLAB using the variable step Runge-Kutta solver ode45.

Functions from the MSS Toolbox [17] were employed in this model to provide the transformation matrix, $\mathbf{J}(\vartheta)$, (described Section III-A) and identification of SSMs to represent radiation affects (described in Section III-C1).

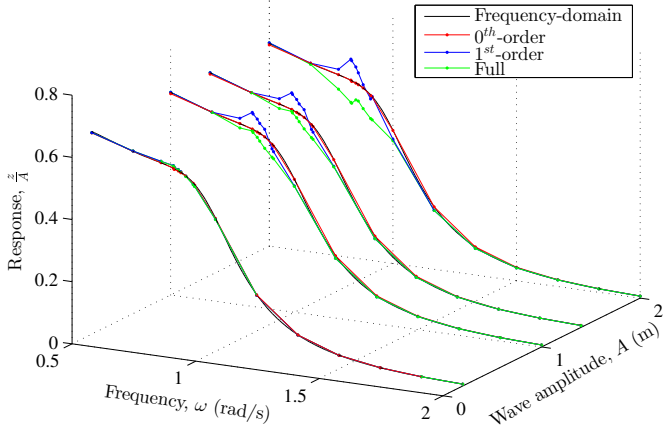


Fig. 5. Heave RAOs for PMPA in waves with heights of $H = 0.2, 1.0, 1.4$ and 2.0 m, all with an angle of incidence of $\beta = 34^\circ$. Response magnitudes are shown from the frequency-domain model and from the time-domain model, using 0^{th} , 1^{st} and full-order coordinate system transformation matrices.

D. Frequency-Domain Model

The frequency-domain equations of motion for a floating body can be defined in the inertial coordinate system illustrated in Fig. 2 by

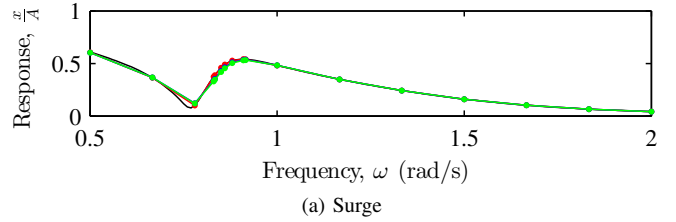
$$\hat{\mathbf{H}}(\omega)\hat{\zeta}(\omega) = \mathbf{J}^{0^{th}}(\vartheta) \left(\mathbf{B}(\omega) + \mathbf{B}_v^L + i\omega(\mathbf{M}_{RB} + \mathbf{A}(\omega)) \right) \dot{\eta} + \frac{\mathbf{G} + \mathbf{C}_m}{i\omega} \dot{\eta} + R_{load} \dot{\eta}. \quad (42)$$

The same hydrodynamic parameters, hydrostatic restoring, mooring, viscous damping, and control strategies discussed above in III-B are employed in this model. Since the frequency-domain requires linearity, no constraints are imposed on the PCC operation. Further, the 0^{th} -order transformation matrix $\mathbf{J}^{0^{th}}(\vartheta)$ is used to adhere to requirements of linearity as discussed above.

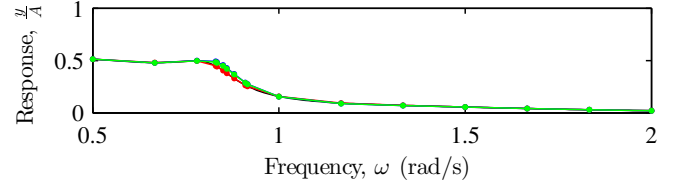
IV. RESULTS

A. Regular Wave Response

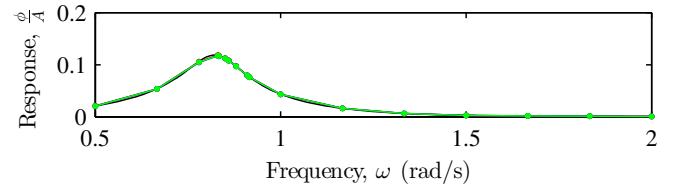
To verify the time-domain model, response amplitude operators (RAOs) were produced for the PMPA when subject to the optimal resistive loading (22) and compared against those obtained using the frequency-domain model subject to the same control. Nonlinear effects were investigated by reviewing the response of the PMPA in waves of increasing height ($H = 0.2, 1.0, 1.4, 2.0$ m), all with an angle of incidence of $\beta = 34^\circ$. The time-domain model was run using each of the 0^{th} -, 1^{st} - and full-order coordinate system transformation matrices discussed in Section III-A. The heave RAOs from this series of simulations are shown in Fig. 5. It is clear from Fig. 5 that the transformation matrix $\mathbf{J}(\vartheta)$ plays a more dominant role in waves of increasing height, as would be expected. The surge, sway, roll and pitch RAOs for the 0.2 m wave series are shown in Fig. 6. As in Fig. 5, the $\mathbf{J}^{0^{th}}(\vartheta)$ time-domain results match the frequency domain results well.



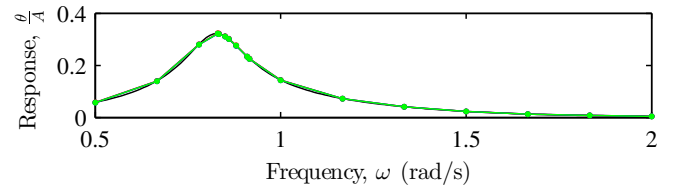
(a) Surge



(b) Sway



(c) Roll



(d) Pitch

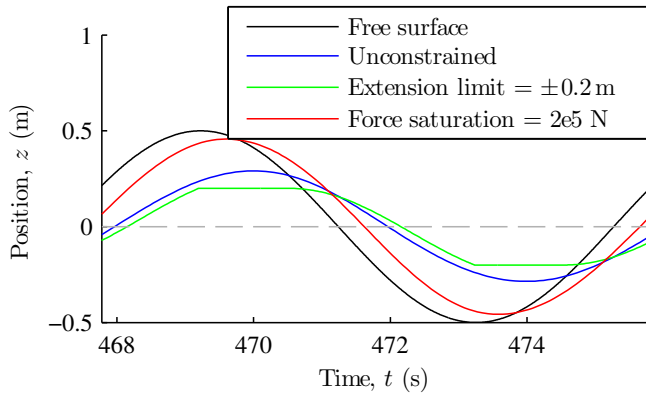
Fig. 6. Surge, sway, roll and pitch RAOs for PMPA in waves with $H = 0.2$ m, with an angle of incidence of $\beta = 34^\circ$. Response magnitudes are shown from the frequency-domain model and from the time-domain model, using 0^{th} -, 1^{st} - and full-order coordinate system transformation matrices. The legend from Fig. 5 applies to the line-series in this figure.

B. Response when subject to PCC constraints

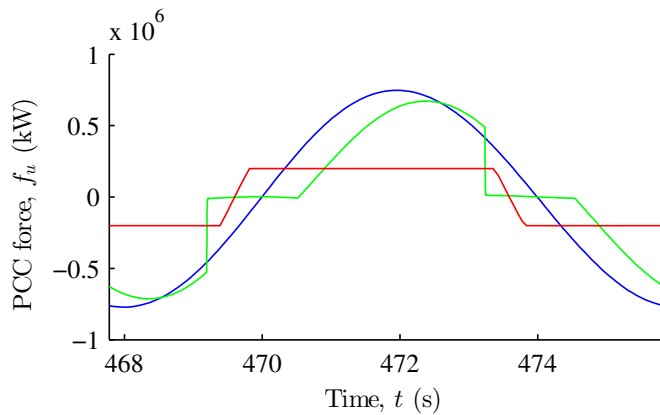
Fig. 7 shows a time history of the PMPA float's position and power absorption during regular waves with $H = 1.0$ m, $\omega = 0.78$ rad/s and $\beta = 0^\circ$. Predictions are shown for three different model constraint configurations (see Section III-B6 for a discussion on the implementation of these constraints):

- *Unconstrained* - No constraints are applied to the model.
- *Extension limit* - The extension of the PCC arm is limited to ± 0.2 m.
- *Force saturation* - The total force applied by the PCC is limited to 2×10^5 N, which is roughly 25% of the optimal resistive load at this frequency.

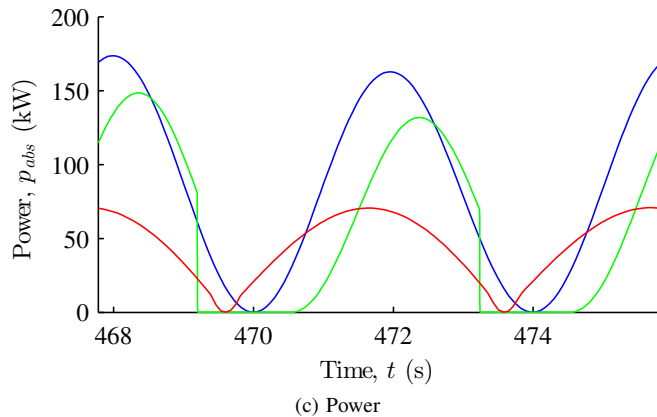
Both the phase and magnitude of the float's response can be observed to change due to the introduction of these constraints. The average absorbed power over the period shown in Fig. 7 was 84.2, 56.3 and 44.7 kW for unconstrained, extension limit and force saturation configurations respectively. Note that the



(a) Vertical position



(b) Force



(c) Power

Fig. 7. PMPA float vertical position, z , force, f_u , and absorbed power, p_{abs} , for regular waves with $H = 1.0$ m and $\omega = 0.78$ rad/s. Predictions shown for unconstrained, PCC extension limited and force saturation limited time-domain model.

response of the extension limit constrained model is highly dependent on the tuning factors of the end-stop function (26) along with the incident wave parameters.

V. CONCLUSION

A time-domain model for a point absorber WEC in six degrees-of-freedom was developed based on Cummins' formulation and verified against a frequency-domain model. A series of simulations were run to show the effect of a posi-

tion linearization assumption. As expected, this assumption loses validity as wave, and motion, amplitude increases. PCC extension limitation and force saturation constraints were demonstrated and shown to affect the response of the device and its power absorption.

Future work will focus on expansion of the time-domain model to give a more complete description of the PMPA and include more of the nonlinearities neglected in (7). Additionally, upcoming experimental testing will allow for hydrodynamic coefficients to be more accurately determined. Further analysis will also be required to better understand the impact of device constraints on power absorption as well as control performance.

ACKNOWLEDGMENTS

This work was funded by the U.S. Department of Energy's Wind and Water Power Technologies Office. Sandia National Laboratories is a multi-program laboratory managed and operated by Sandia Corporation, a wholly owned subsidiary of Lockheed Martin Corporation, for the U.S. Department of Energy's National Nuclear Security Administration under contract DE-AC04-94AL85000.

REFERENCES

- [1] WAMIT, 7th ed., 2012. [Online]. Available: <http://www.wamit.com/manual.htm>
- [2] T. I. Fossen, *Guidance and control of ocean vehicles*. Chichester; New York: Wiley, 1994.
- [3] —, *Handbook of marine craft hydrodynamics and motion control*. Chichester, West Sussex: Wiley, 2011.
- [4] W. E. Cummins, "The impulse response function and ship motions," Department of the Navy, David Taylor Model Basin, Bethesda, MD, Tech. Rep. DTNSDR 1661, 1962. [Online]. Available: <http://dome.mit.edu/handle/1721.3/49049>
- [5] F. T. Ogilvie, "Recent progress towards the understanding and prediction of ship motions." in *Proceedings of the 6th Symposium on Naval Hydrodynamics*, Washington DC, 1964.
- [6] J. N. Newman, *Marine hydrodynamics*. Cambridge, Massachusetts: MIT Press, 1978.
- [7] J. Morison, J. Johnson, S. Schaaf *et al.*, "The force exerted by surface waves on piles," *Journal of Petroleum Technology*, vol. 2, no. 05, pp. 149–154, 1950. [Online]. Available: <https://www.onepetro.org/journal-paper/SPE-950149-G>
- [8] D. Bull and E. Johnson, "Optimal resistive control strategy for a floating OWC device," in *Proceedings of the 10th European Wave and Tidal Energy Conference*. Aalborg, Denmark: Technical Committee of the European Wave and Tidal Energy Conference, 2013. [Online]. Available: <http://energy.sandia.gov/wp/wp-content/gallery/uploads/SAND2013-6198c.pdf>
- [9] Z. Yu and J. Falnes, "State-space modelling of a vertical cylinder in heave," *Applied Ocean Research*, vol. 17, no. 5, pp. 265–275, Oct. 1995. [Online]. Available: <http://www.sciencedirect.com/science/article/pii/0141118796000028>
- [10] J. Falnes, *Ocean Waves and Oscillating Systems*. Cambridge; New York: Cambridge University Press, 2002.
- [11] J. Hals, J. Falnes, and T. Moan, "A comparison of selected strategies for adaptive control of wave energy converters," *Journal of Offshore Mechanics and Arctic Engineering*, vol. 133, no. 3, p. 031101, March 2011. [Online]. Available: <http://offshoremechanics.asmedigitalcollection.asme.org/article.aspx?articleid=1456895>
- [12] E. Kristiansen, Å. Hjulstad, and O. Egeland, "State-space representation of radiation forces in time-domain vessel models," *Ocean Engineering*, vol. 32, no. 1718, pp. 2195–2216, Dec. 2005. [Online]. Available: <http://www.sciencedirect.com/science/article/pii/S0029801805000946>

- [13] T. Perez and T. I. Fossen, "Time- vs. frequency-domain identification of parametric radiation force models for marine structures at zero speed," *Modeling, Identification and Control*, vol. 29, no. 1, p. 119, 2008. [Online]. Available: <http://www.mic-journal.no/PDF/2008/MIC-2008-1-1.pdf>
- [14] T. Duarte, A. Sarmiento, M. Alves, and J. Jonkman, "State-space realization of the wave-radiation force within FAST," in *Proceedings of the 32nd International Conference on Ocean, Offshore and Arctic Engineering*. Nantes, France: ASME, 2013. [Online]. Available: <http://www.nrel.gov/docs/fy13osti/58099.pdf>
- [15] R. Taghipour, T. Perez, and T. Moan, "Hybrid frequency-time domain models for dynamic response analysis of marine structures," *Ocean Engineering*, vol. 35, no. 7, pp. 685–705, May 2008. [Online]. Available: <http://www.sciencedirect.com/science/article/pii/S0029801807002363>
- [16] T. Duarte, *SS Fitting Theory and User Manual*, Golden, Colorado, 2013. [Online]. Available: http://wind.nrel.gov/designcodes/preprocessors/SS_Fitting/
- [17] MSS. (2010) Marine systems simulator. [Online]. Available: <http://www.marinecontrol.org>